Thermogravimetric analysis of modified hematite by methane (CH_4) for chemical looping combustion: a global kinetics mechanism

Esmail R. Monazam[2], Ronald W. Breault[*1], Ranjani Siriwardane[1], Duane D. Miller[3]

[1]National Energy Technology Laboratory
U. S. Department of Energy
3610 Collins Ferry Rd.
Morgantown, West Virginia 26507-0880
[2]REM Engineering Services, PLLC
3537 Collins Ferry Rd.
Morgantown, West Virginia 26505
[3]URS Energy & Construction, Inc.
3610 Collins Ferry Rd.
Morgantown, WV. 26505

Iron oxide (Fe_2O_3) or in its natural form (hematite) is a potential material to capture CO_2 through the chemical-looping combustion (CLC) process. It is known that magnesium (Mg) is an effective methyl cleaving catalyst and as such it has been combined with hematite to assess any possible enhancement to the kinetic rate for the reduction of Fe_2O_3 with methane. Therefore, in order to evaluate its effectiveness as a hematite additive, the behaviors of Mg-modified hematite samples (hematite –5% $Mg(OH)_2$) have been analyzed with regard to assessing any enhancement to the kinetic rate process. The Mg-modified hematite was prepared by hydrothermal synthesis. The reactivity experiments were conducted in a thermogravimetric analyzer (TGA) using continuous stream of CH_4 (5, 10, and 20%) at temperatures ranging from 700 to 825 ^oC over ten reduction cycles. The mass spectroscopy analysis of product gas indicated the presence of CO_2, H_2O, H_2 and CO in the gaseous product. The kinetic data at reduction step obtained by isothermal experiments could be well fitted by two parallel rate equations. The modified hematite samples showed higher reactivity as compared to unmodified hematite samples during reduction at all investigated temperatures.

Introduction

Carbon dioxide ($CO_{2)}$ has been identified as a major green house gas and its concentration has been increasing in the atmosphere over the past one hundred years likely due to the combustion of fossil fuels such as coal, petroleum, and natural gas and may lead to disastrous changes in our planet's climate. To address this possible effect, the United States, through the Department of Energy as well as other countries are looking at alternative ways to reduce the atmospheric CO_2 concentration. The available CO_2 capture technologies are energy intensive and costly [1-3]. As a result, an alternative process such

* Corresponding author: Tel. 304-285-4486; fax:304-285-4403; email: Ronald.breault@netl.doe.gov

as chemical-looping combustion (CLC) has been proposed for the reduction of CO_2 emissions[4, 5].

Chemical looping processes data back to the early 1900's where the technique was used for coal gasification through the steam-iron process. More recently, in the early 1980's the technique was applies to combustion by Richeter and Knoche[4], who suggested oxidizing the fuel by an oxygen carrier, i.e. an oxygen-containing compound, in a flameless combustion process instead of oxidizing the fuel with oxygen from the combustion air. The reduced oxygen carrier is then reoxidized by air in a second reactor and recirculated to the first reactor. In this way, fuel and air are never mixed and the fuel oxidation products CO_2 and water leave the system undiluted by excess air. Pure CO_2 is produced after condensation of water vapor and removal of the liquid water[6]. Thus, the CLC process does not require an expensive CO_2 separation process.

The CLC-process has been successfully demonstrated using gaseous fuel with different oxygen carriers in several prototype units based on interconnected fluidized-beds[7–17]. An overview of literature concerning CLC is given by Lyngfelt et al.[18] or Hossain and de Lasa[19]. The major part of the work concerning CLC has so far been with gaseous fuel, such as natural gas or methane, when methane is used as a reducing agent CO_2 emission are less compared to other fuels and contamination emissions are negligible.
Since the oxygen carriers are subjected to reduction followed by subsequent oxidation, they are subjected to important structural changes making necessary the use of a support that, presumably, remains inactive in the two involved stages. The support not only imparts a high mechanical strength to the overall carriers but also a high dispersion of the active phase embedded in the porous support[20]. Different metal oxides have been proposed as possible candidate for the CLC process[21]; the four most studied supported oxygen carriers in descending order by reactivity are $NiO > CuO > Mn_2O_3 > Fe_2O_3$ while suitable supports are alumina, silica, zirconia and titania[21-25].
.
Some of these oxides have a number of disadvantages, for example the use of Ni-based carries introduces a high level of toxicity into the environment and the low melting point of elemental copper (1362 K) creates process design issues when used in high temperature applications. Furthermore, the cost of these two raw materials is relatively high. Alternatively, Fe_2O_3 is cheap and environmentally friendly, but has generally a lower reactivity with methane compared with Ni- and Cu-based systems. Iron oxide and metallic iron are also employed as catalysts in a number of important chemical processes. In its application as catalyst, the degree of reduction of the iron species is highly important. Additionally, the melting points of all involved iron compounds in the two stages are very high. Consequently, iron oxides are materials potentially suitable as oxygen carriers for a CLC of methane but the performance must be assessed in multicycle reactor tests. We have previously reported kinetic analysis for the methane CLC reaction with pure hematite[26]. Therefore, the objective of this paper is thus to understand the kinetic parameters on the performance of MgO-supported hematite (Fe_2O_3) with different MgO loading (5 and 25%), as oxygen carriers for a CLC of methane using TGA. The effect of temperature and gas concentration was studied.

According to our best knowledge this is the first kinetic investigation for MgO-supported hematite oxygen carriers for CLC.

Experimental

Thermogravimetric Analysis (TGA) Apparatus

A sketch of the reactor unit a TA Model 2050 thermo gravimetric analyzer[26], is shown in Figure 1. A sample is placed on the pan (5-mm deep and 10-mm diameter) which is centered in the gas feed and gas exit ports. The port at the bottom is closed. Sweep gas keeps the balance electronics in an inert environment and enters the reaction chamber at the top. A typical TGA experimental data on weight changes during reduction/oxidation for cyclic tests at a given temperature are illustrated in Figure 2. The samples of Mg-modified hematite were placed in a 5-mm deep and 10-mm diameter quartz crucible. For a typical test, about 80 mg of the modified hematite sample was heated in a quartz bowl at a heating rate of 10 °C/min under N_2 gas at a flow rate of 100 cm^3/min. The analysis arriving at these conditions and showing that there is no mass transfer or mixing issues confounding the analysis is presented in detailed by Monazam et al.[26].

The sample temperature was maintained isothermally for 20 minutes prior to the reduction and oxidation cycles. The reduction−oxidation cycles were conducted within the temperature range 700−825 °C for 10 cycles, using 5%, 10%, and 20% CH_4 concentrations in N_2 for the reduction segment and and air at a total flow rate of 100 cm^3/min was used during oxidation. Reduction reaction times were set at 45 min, and oxidation reaction times were 30 min for all experiments. The system was flushed with ultra-high pure nitrogen for 10 minutes before and after each reaction segment.

The system was flushed with ultra-high pure nitrogen for 10 minutes before and after each reaction segment. The concentrations of CH_4, CO_2, H_2O, H_2, CO, and O_2 from the exit gas stream of the reactor were analyzed using a mass spectrometer. The mass spectrometer is manufactured by Pfeiffer Omnistar GSD-301.
The oxygen carrier preparations are described elsewhere[27]. The 5 wt% and 25 wt% MgO-modefied hematite oxygen carriers were prepared from commercial $Mg(OH)_2$ (Aldrich), dolomite (Aldrich), and magnesium nitrate (Aldrich). The pure magnesium oxide material was obtained by calcining the $Mg(OH)_2$ in a furnace at 800 ^oC. For comparison purposes, 5 wt% and 25 wt% Al_2O_3/Hematite were also prepared by the impregnation method. Following calcination at 800 ^oC for 3 h, the oxygen carrier samples were sieved to 100-300 micron. The BET surface area and pore size of the oxygen carriers were measured using a Micromeritics ASP-2020 apparatus and results are presented in Table 1. The Michigan hematite used for these studies was supplied by Ward's Natural Science Rochester, NY. The UHP grade CH_4, used for the reduction cycle, was obtained from Matheson Tri-gas. The N_2/O_2 (Air) used for the oxidation cycle was obtained from Butler Gas Products Co. Inc.

Results and Discussion

Modefied hematite was reduced at different temperature (700-825^{o}C) for various CH_4 concentrations (5%- 20%) for times up to 30 min. The extent of reduction calculated using the following equation:

$$X = \frac{m_o - m(t)}{m_o - m_f} \qquad (1)$$

where *m(t)* is the instantaneous weight of the solid during the exposure to CH_4. Parameters m_o and m_f are initial and final weight of the sorbent, respectively. In this study, the initial weight was considered as the weight of modified hematite and final weight as the weight of either Fe_3O_4, or FeO and or Fe (depends on degree of reductions). In this study, m_f is considered as the mass of FeO and 100% conversion means that the modified hematite was all converted to FeO (wüsite). Theoretical weight decrease corresponding to transformation of Fe_2O_3 into Fe_3O_4 is 3.3 wt % and of Fe_2O_3 into FeO and Fe corresponds to weight decrease of 10 wt% and 30 wt% respectively.

Figure 3 illustrates the extent of reduction as a function of time obtained at different temperature with 10% CH_4 concentration. The results reveal that the degree of reduction increases with temperature and time. At the beginning the reduction proceeds rapidly up to about 5 min, after which only gradual increase in reduction is observed.
It should be noted that only fewer chosen data points are shown at each temperature for clear illustration of the trend of the curves in Figure 3. The solid lines represent the model fit to experimental data that will be discussed later.
Figure 3 also shows there is a marked decrease in the extent of reduction time when temperature is raised from 700 to 750^{o}C. This is substantiated by the decrease in the extent of reduction time to form Fe_3O_4 from 5 minutes at 700^{o}C to about 2.5 minutes in 750^{o}C. By increasing the temperature to 800^{o}C, the reduction time decreases further but the difference in time is less pronounced than that observed between 700 and 750^{o}C. These results suggest at 700^{o}C, the energy provided is inadequate to achieve reduction at a fast rate for modified hematite.

Figures 4 and 5 show the product gas concentration (as measured by mass spectrometer) variation as a function of time at 825 ^{o}C, with inlet methane concentrations of both10 and 20%. The data in Figure 4 also shows that the CH_4 concentration at the outlet increases rapidly, reaches a temporal maximum, decreases slightly and then increases slowly to the final value. The temporal maxima is reached at the same time that the CO_2 begins to decrease. Then CH_4 concentrations continue to increase, whilst a certain amount of CO (Figure 5) and H_2, which is associated with the thermodynamic limitation of Fe_2O_3 to convert CH_4 fully to CO_2 and H_2O, was observed. After about two minutes, the production of CO_2 concentration diminishes completely whereas the concentration of CO and H_2 decreases slowly, indicating that the reducing process was mainly selective towards the formation of CO and H_2 at the latter stage of the reduction process.

During the oxidation phase, after air was introduced into the reactor, a peak of CO_2 (Figure 6) immediately appeared in the reactor outlet gases. This indicated that the carbon deposited during the reduction phase was oxidized to CO_2 during the oxidation phase.

Figure 7 shows the average carbon formation calculated from the CO_2 formed during oxidation (Figure 6) at different temperatures and at various CH_4 inlet concentrations. The carbon deposition increased slightly with both increasing temperature and increasing methane concentration, while the ratio of carbon deposited to amount of inlet carbon from CH_4 increases with temperature and decrease with increasing methane concentration.
This behavior is readily explained by the fact that the driving force for CH_4 decomposition reaction to form C and H_2 increases with increasing temperature. The carbon deposition was assumed to occur evenly over the 30 min reduction cycle when the weight loss during reduction was corrected. However, it is likely that carbon deposition occurred later in the process. Overall, carbon formation would have an insignificant effect on the results particularly during the lower residence times where the process is envisioned to operate.

Cho et al.[28] mentioned two possible mechanisms of carbon formation during reduction: methane decomposition and the Boudouard reaction. Kinetically, both of these are slow in the absence of a catalyst. However, metals such as FeO and Fe could act as a catalyst. Carbon deposition may have been initiated when there was sufficient FeO/Fe present, i.e. towards the end of the reduction phase. These results imply that there is a competition between direct reaction of CH_4 with Fe_2O_3 /Fe_3O_4/FeO to from CO_2/CO and cracking of CH_4 to form C and H_2 in the presence of FeO/Fe metal acting as a catalyst. The CH_4 cracking at high temperature in the presence of FeO/Fe metal could have lead to the formation of CO and H_2.

Kinetic Models

The conversion date during gas/solid reactions is a useful tool to access the gas-solid kinetics. Generally, the reaction rate of gas-solid reactions is a function of both temperature and conversion (*X).* For reaction kinetics under isothermal conditions, constant gas flow rate and at a given inlet gas concentration, the conversion rate can be expressed as;

$$\frac{dX}{dt} = k(T)\, f(X) \qquad (2)$$

where *t* is the time, *T* is the temperature, *X* is the extent of conversion, *f (X)* is the reaction model (Table 2). In equation (2), *k(T)* is the Arrhenius rate constant, which is given as:

$$k(T) = A\exp\left(\frac{-E}{RT}\right) \qquad (3)$$

where *R* is the gas constant, and *A* and *E* are the pre-exponential factor and the activation energy, respectively.

For reaction kinetics under isothermal conditions, equation (2) can be analytically integrated to yield:

$$g(X) = \int_0^X \frac{dX}{f(X)} = k(T)t \qquad (4)$$

where *g(X)* is an integral mathematical expression related to a mechanisms of solid phase reactions.
As shown in table 2, Five groups of mathematical expressions: (P1, P2, P3, P4), (R1, R2, R3), (F1, F3/2, F2, F3), (A3/2, A2, A3, A4), and (D1, D2, D3, D4) describe power law, contraction, chemical reaction, nucleation and diffusion mechanisms, respectively. Table 2 also summarizes these kinetic models as well as their algebraic expressions[29].

The mathematical expressions *g(X)* describing the possible reaction mechanisms together with the experimental *X* and t values corresponding to a fixed temperature were inserted in Eq. (4). The values of kinetic constant rate *k* can be determined at different temperatures from the slope of the straight line obtained by plotting *g(X)* against time. As illustrated by Figure 7, none of the expressions listed in Table 2 provided straight line fitting parameters indicating that the CH4/modified hematite reactions did not follow the mechanisms defined in these models. Therefore, an alternative procedure, the isothermal isoconversional method[30], was used to verify the energy value variation related to the multi-step in the experimental temperature range.

From isothermal TGA curves, a set of temperature *T* and *t* values were obtained for fixed values of *X*. Substituting $k=A\ exp(-\ E/RT$ in equation (4) one can obtain;

$$g(X) = A\exp\left(\frac{-E}{RT}\right)t \qquad (5)$$

By taking the logarithm and rearranging it, one can obtain;

$$\ln t = (-\ln A + \ln g(X)) + \frac{E}{RT} \qquad (6)$$

By plotting ln*t* versus *1/T* according to equation 6, the activation energies were found at any given *X* values from the slope of a regression line. Knowledge of the dependence activation energy on *X* assists in both detecting multi-step processes and drawing certain mechanistic conclusions[30]. If activation energy does not vary significantly with *X*, the process can be adequately described as single-step kinetics. If activation energy varies with *X*, the process has to be described as multiple step kinetics.

Figure 9 provides the results of the model-free isoconversional computations using CH_4 concentration of 20%, 10% and 5%. With increasing *X*, the activation energy initially decreased from 147 to 50 kJ/mole (0.05<X<0.3) (the average E_a value is estimated to be 82±28. kJ/mole) and then increased from 50 to 155 kJ/mole (0.3<X<0.5) (average E_a value is estimated to be 100±31. kJ/mole).

Therefore, the application of the isoconversional method to isothermal data, results in activation energies that vary strongly with the extent of reaction. Such dependencies are an unmistakable indication of the process complexity[31]. In particular, the dependencies obtained suggest that the process involves at least two reactions with different activation energies, whose values can be approximately estimated as the extreme values that limit the region of the *E(X)* variation.

Reaction Schemes

From these results it can be observed that the reaction of modified hematite with CH_4 follow multi-step kinetics. In this study, we have chosen a simple multi-step process that involves two parallel or series independent reactions.

$$\begin{aligned} A &\xrightarrow{k_1(T)} product \\ B &\xrightarrow{k_2(T)} product \end{aligned} \qquad (7)$$

While simple, this mechanism may reasonably approximate the process of conversion of a substance that exist in two isomeric forms, or a conversion of a reactant that simultaneously exists in two phases or a conversion of a solid by two separate paths to different products. As Figure 9 indicated that the activation energy decreases as conversion increases (0.05<X<0.3) and then increases with further increase in conversion (0.3<X<0.5). The equations involved in isothermal processes are the following[26,32]:

• Parallel:

$$\frac{X_t}{X_\infty} = w_1(1-e^{-a_1 t^{n_1}}) + w_2(1-e^{-a_2 t^{n_2}}) \qquad (8)$$

• Series:

$$\frac{X_t}{X_\infty} = w_1\left(\frac{1}{1-e^{-a_1 t^{n_1}}}\right) + w_2\left(\frac{1}{1-e^{-a_2 t^{n_2}}}\right) \qquad (9)$$

Where:
a_1=nucleation rate constant for the first mechanism (min.$^{-n_1}$),
a_2=nucleation rate constant for the second mechanism (min.$^{-n_2}$),
n_1= shape parameter for the first mechanism,
n_2= shape parameter for the second mechanism,
t=time (min),
w_1=weight factor for the first mechanism,
w_2= weight factor the second mechanism,
X_t=total conversion at any time t,
X_∞=equilibrium conversion.

For *n* values of 1, the equation (8) reduces to simple first order reaction kinetics. The equations (8) and (9) corresponds to two different nucleation or growth processes occurring in parallel or series, with the relative importance of each manifested by the value of the weight factors w_1 and w_2 where $w_1 + w_2 = 1$.[31] Note that equations (8) and (9) describe the isothermal processes, so $a(T)$ is a constant at a given temperature. As illustrated by Figure 10 reaction model with reactions in series did not produce comparable results with experimental data. However, the data from the reaction model with parallel reaction were very compatible with the experimental data. Therefore, in this study, reaction model in parallel was used for reduction of modified hematite using methane.

For a given temperature, values of X_∞, w_2, a_1, a_2 , $n_1$and $n_2$were determined by curve fitting the rate data of Figure 3 with the parameters in equation (8) using TABLECURVE available from Statistical Package for the Social Sciences. The values determined for the shape parameters, n_1, range from 0.6 to 1.6 for all the temperatures and all the CH_4 concentrations; the average value of n_1 was 0.97± 0.3 (95% CL). The values determined for the shape parameters, n_2, range from 0.85 to 1.7 for all the temperatures and all the CH_4 concentrations; the average value of n_2 was 1.13± 0.32 (95% CL). The observed value of n_1= 0.97 and n_2= 1.13 was very close to the value of $n_1 = n_2 = 1$ that defines the pseudo-first order rate expression. In order to simplify the analysis, value of $n_1 = n_2 = 1$ was used. The values of X_∞, w_2, a_1 and a_2 were recalculated based on the approximation of $n_1 = n_2 = 1$ for every set of conversion data at different temperatures and CH_4 concentrations. The addition of the magnesium to the hematite has changed the reaction model to first order from nucleation and growth[26] model which was observed for hematite. Since the nucleation and growth mechanism has the diffusion controlled process at the early stage of conversion, the physical properties, particularly the BET surface areas (Table 1) were evaluated to understand the possible reason for this change to first order kinetics for modified hematite as compared to unmodified hematite. Basically, no difference was found as both materials had BET surface areas less than 1.0 m^2/g. However, the pore diameter of the modified hematite increased by a factor of nearly five as compared to un modified hematite. This may have an effect on reducing the diffusion into the material and is contributed for the change in mechanism from nucleate and growth for hematite to first order for the Mg-modified hematite.

The effect of reaction temperature on the conversion of modified hematite during the 30 min reduction is shown in Figure 3. It should be noted the final mass (m_f) corresponding to conversion value of 1 was considered as mass of FeO. Increasing the temperature increased the reaction rate.

The comparison of the experimental modified hematite conversion data (X) and the conversion based on parallel model as presented in equation (8) (using $n_1 = n_2 = 1$) is also illustrated in Figure 3 at different temperatures. It should be noted the final mass (m_f) corresponding to conversion value of 1 was considered as mass of FeO. The model data and experimental data agree over the entire conversion time with overall variance (R^2) greater than 99.9%. When fitting non-linear equations with a large number of

parameters, it is prudent to consider how sensitive the trend is to the choice of input parameters, and whether equally good fits could be achieved with different sets of parameters. Indeed, it was found out the unknown parameters did not vary with different initial choices. The data in Figure 3 also shows that the rate of reduction of modified hematite increases as the reaction temperature is increased.

The parallel reactions, R_1 and R_2, which are first order curves, represent two processes of reactions occurring simultaneously, but with different time dependence. The comparison of the R_1 and R_2 parallel reaction model and experimental data is illustrated in Figure 11. The curve R_1 which represents reaction 1 has a faster time response than reaction 2 (curve R_2), and curve 3 is the sum of the two reactions R_1 and R_2. As time progresses, reaction 1 and 2 reach steady state at different degrees of reduction. That is, if process 1 alone were contributing to the bulk reaction, at long times the degree of reduction would be product of $w_1$and X_∞. With both reactions contributing, the degree of reduction at long times is product of (w_1+w_2) and X_∞. Figure 11 illustrates that in the initial portion of the reaction, the time dependence of total reaction, curves (R_1+R_2), and is dominated by reaction R_1. At long times, the total reaction (R_1+R_2) is dominated by reaction R_2. Hence, the reaction 2 will have little influence on the initial part of the reduction process.

The effects of reaction temperature on the conversion of each reaction (R_1 and R_2) during the 30 min reduction are shown in Figure 11. The data indicates that the reaction rates of both reactions R_1 and R_2 increase with increasing temperature.

In order to determine the rate controlling mechanism, the value of apparent activation energy was calculated from Arrhenius equation for n=1;

$$k = a = k_0 e^{\frac{-E}{RT}} \qquad (10)$$

Where k is the reduction rate constant, k_0 is the frequency factor, R is the gas constant and T is the absolute temperature. The linear regression of the experimental data of ln k against 1/T determines E/R. A plot of $ln\ k$ vs 1/T for both reduction reaction, R_1 and R_2 for modified hematite are shown in Figure 12 for all inlet CH_4 concentrations (15, 20, and 35%). The error bars lengths are defined by the range of the data at each temperature. The pre-exponential factor, k_0, and activation energy, E, were obtained from the intercept and slope of the straight line of $ln\ k$ vs 1/T for a given CH_4 concentration. The apparent activation energies for both reactions R_1 and R_2 were estimated to be 50.2 ± 0.36 and 64.8 ± 1.14 kJ/mole, respectively. These values of E_1 and E_2 lie inside the limits of the activation energy as a function of conversion.

These activation energies are comparable with values obtained by other investigators.[33, 34] Abad et al.,[33] reported a value of 49 kJ/mole for the reaction rate of methane combustion over Fe45Al-FG. Moghtaderi and Song[34] reported activation energy of 53 kJ/mole for reduction of iron ore with CH_4.

The values of shape factor indicate that as CH_4 concentration increases the value of w_2 increases linearly. However, as temperature increases, the value of w_2 decreases linearly.

A linear fit to the functionality gave a R^2 of greater than 85%. Combining all the values of w_2 for different temperatures and CH_4 concentrations, the following equation is obtained;

$$w_2 = -0.828 + .0017 \times T(^oC) + 0.1404 \times y_{CH_4} \quad (11)$$

The equilibrium conversion, X_∞, for all the CH_4 concentrations as a function of reaction temperatures indicates that the value of X_∞ increases linearly with increase in both concentrations and temperatures. A linear fit to the functionality gave a R^2 of greater than 82%. Combining all the values of X_∞ for different temperatures and CH_4 concentrations, the following equation is obtained;

$$X_\infty = 1.3663 - \frac{417951.51}{T^2(^oC)} + 18.05 \times y_{CH_4}^3 \quad (12)$$

An expression for the reaction rate, *dX/dt*; can be derived by differentiating equation (8) with respect to t, at constant temperature, as follows:

$$\left.\frac{dX_1}{dt}\right|_{R_1} = k_1\left(w_1 X_\infty - X_1\right) \quad (13)$$

and

$$\left.\frac{dX_2}{dt}\right|_{R_2} = k_2\left(w_2 X_\infty - X_2\right) \quad (14)$$

Therefore, the total rate is summation of equations (13) and (14) as;

$$\left.\frac{dX_t}{dt}\right|_{R_1+R_2} = k_1(w_1 X_\infty - X_1) + k_2(w_2 X_\infty - X_2) \quad (15)$$

Combining all the values of k_1 and k_2 for different CH_4 concentrations and placing them in Eq. 10, the following global *k*'s equation were obtained

$$k_1 = 383.88\, y_{CH_4}^{0.182} e^{\frac{-6040.3}{T}} \quad (16)$$

and

$$k_2 = 144.64\, y_{CH_4}^{0.272} e^{\frac{-7798}{T}} \quad (17)$$

The coefficients were taken as the average of the upper and lower limits for 95% confidence limits.

The individual rate-time data obtained at different temperatures (700−825 °C) using equations (13) and (14) are also shown in Figures 12 for reactions R_1 and R_2. As shown in Figure 13, the rate−time curves for R_1 and R_2 shows that the maximum rate when times equal to zero at all temperatures. This is consistent with rate data of kinetically controlled

reaction in which the maximum rate occurs when time equal to 0, or when *n* equal to 1 in the Avarami equation. Data in Figures 13 also shows that the value of maximum rate increases with the increasing temperature for both R_1 and R_2.

The possible reaction mechanism deduced from our other experimental data is summarized below[26,27].

Methane decomposition and reduction of modified hematite to Fe_3O_4

$$3CH_4 \rightarrow 3C + 6H_2 \qquad \Delta H^o_{r,800C} = 268.34\,kJ/mol \quad (18)$$

$$CH_4 + 12Fe_2O_3 \rightarrow 8Fe_3O_4 + CO_2 + 2H_2O \qquad \Delta H^o_{r,800C} = 164.1\,kJ/mol \quad (19)$$

$$3C + 12Fe_2O_3 \rightarrow 8Fe_3O_4 + CO_2 + 2CO \qquad \Delta H^o_{r,800C} = 346.2\,kJ/mol \quad (20)$$

$$H_2 + 3Fe_2O_3 \rightarrow 2Fe_3O_4 + H_2O \qquad \Delta H^o_{r,800C} = -6.75\,kJ/mol \quad (21)$$

$$4CH_4 + 27Fe_2O_3 \rightarrow 18Fe_3O_4 + 2CO_2 + 2CO + 3H_2O + 5H_2 \quad \Delta H^o_{r,800C} = 771.86\,kJ/mol \quad (R_1) \quad (22)$$

Methane decomposition and reduction of Fe_3O_4 to FeO

$$2CH_4 \rightarrow 2C + 4H_2 \qquad \Delta H^o_{r,800C} = 178.9\,kJ/mol \quad (23)$$

$$CH_4 + 4Fe_3O_4 \rightarrow 3FeO + 2H_2O + CO_2 \qquad \Delta H^o_{r,800C} = 377.9\,kJ/mol \quad (24)$$

$$2C + 3Fe_3O_4 \rightarrow 9FeO + CO_2 + CO \qquad \Delta H^o_{r,800C} = 377.5\,kJ/mol \quad (25)$$

$$H_2 + Fe_3O_4 \rightarrow 3FeO + H_2O \qquad \Delta H^o_{r,800C} = 46\,kJ/mol \quad (26)$$

$$3CH_4 + 8Fe_3O_4 \rightarrow 24FeO + 2CO_2 + CO + 3H_2O + 3H_2 \quad \Delta H^o_{r,800C} = 981\,kJ/mol \quad (R_2) \quad (27)$$

$$7CH_4 + 27Fe_2O_3 \rightarrow 10Fe_3O_4 + 24FeO + 4CO_2 + 3CO + 6H_2O + 8H_2 \qquad \Delta H^o_{r,800C} = 1752.9\,kJ/mol \quad (28)$$

It is significant to note that the reaction order obtained for two reactions (0.182 for R_1 (Eq. 16) and 0.272 for R_2 (Eq. 17) are similar to the stoichiometric ratios of CH_4 to Fe_2O_3 in equations 22 and 27, respectively.

Figure 15 illustrate the enhancement achieved with the Mg-modified hematite by observing the degree of reduction between Mg-modified hematite and unmodified hematite using 20% methane at 750 and 800^{o}C. At residence times of 5 minutes and greater, the conversion of the Mg-modified hematite is nearly double that for the unmodified. What is particularly exciting is the fivefold increase in the conversion at a residence time of 2 minutes going from a conversion of 10% for the unmodified to 50% for the Mg-modified hematite. It is also clear that the modified hematite samples showed higher reactivity in compared to unmodified hematite samples during reduction at all

investigated temperatures. The magnesium changes the kinetic mechanism for the reaction from nucleation-diffusion to first order. In doing so, the conversion is doubled at any given time.

Summary

In this study, a rigorous approach has been taken to describe the kinetics of the reduction of MgO modified hematite in methane atmosphere over the range of 700–825 ^{o}C and with three CH_4 concentrations: 5, 10, and 20%. Experimental results suggested that, within the range of temperatures studied, the kinetics of reduction of modified hematite consists of two competing 1st order kinetic rates. These results suggest that the reduction of modified hematite (Fe_2O_3) proceed via a two simultaneous reactions. The activation energy value evaluated are 50.2 ± 0.36 for reaction R_1 and 64.8 ± 1.14 kJ/mole for reaction R_2. A series of possible reaction mechanisms of R_1 and R_2 have been identified. The reaction rates for both reaction increases as temperature was increased. The magnesium changes the kinetic mechanism for the reaction from nucleation-diffusion to first order and doubles the conversion for a given time.

Acknowledgment

The authors acknowledge the Department of Energy for funding the research through the office of Fossil Energy's Gasification Technology and Advanced Research funding programs. Special thanks go to Hanjing Tian and Thomas Simonyi of URS Energy & Construction, Inc. for their assistance with experimental work and data.

DISCLAIMER

References

(1) Akai, M.; Kagajo, T.; and Inoue, M. Performance evaluation of fossil power Plant with CO_2 recovery and a sequestering system. *Energy Convers. Mgmt*, **1995**, 36, 801.

(2) Kimura, N.; Omata, K.; Kiga, T.; Takano, S.; and Shikisma, S. The characteristics of pulverized coal combustion in O_2/CO_2 mixtures for CO_2 recovery. *Energy Convers. Mgmt.* **1995**, 36,805.

(3) Ishida, M.; and Jin, H. CO_2 recovery in a power plant with chemical looping combustion. *Energy Convers. Mgmt.* **1996**, 38, 187.

(4) Richter, H.J.; and Knoche, K.F. Reversibility of combustion processes. ACS Symposium Series, **1983**, 235, 71.

(5) Ishida, M.; Zheng, D.; and Akehata, T. Evaluation of a chemical-looping-combustion power-generation system by graphic exergy analysis. *Energy-The Int. Journal*, **1987**, 12, 147.

(6) Xiang, W.G.; and Chen, Y.Y. Hydrogen and electricity from coal with carbon dioxide separation using chemical looping reactors. *Energy Fuels*, **2007**, 21, 2272.

(7) Lyngfelt, A.; and Thunman H. Construction and 100 h of operational experience of a10-kW chemical-looping combustor. In: Carbon dioxide capture for storage in deep geologic formations – results from the CO_2 capture project, vol. 1. 2005. p. 625–45.

(8) Lyngfelt, A.; Kronberger, B.; Adánez, J.; Morin, J-X.; and Hurst, P. The GRACE project. Development of oxygen carrier particles for chemical-looping combustion. Design and operation of a 10 kW chemical-looping combustor. In: Proceedings of The 7th International Conference on Greenhouse Gas Control Technologies. Canada: Vancouver; 2004.

(9) Ryu, H-J.; Jin, G-T.; Bae, D-H.; and Yi, C-K. Continuous operation of a 50 kWth chemical looping combustor: long-term operation with Ni- and Co-based oxygen carrier particles. Presented at the 5th China–Korea joint workshop on clean energy technology, October 25–28. China: Qingdao University; 2004. p. 221–30.

(10) Abad, A.; Mattisson, T.; Lyngfelt, A.; and Rydén, M. Chemical-looping combustion in a 300W continuously operating reactor system using a manganese-based oxygen carrier. *Fuel*, **2006**, 85(9),1174.

(11) Johansson, E.; Mattisson, T.; Lyngfelt, A.; and Thunman, H. A 300W laboratory reactor system for chemical-looping combustion with particle circulation. *Fuel*, **2006**, 85 (10–11), 1428.

(12) de Diego, L. F.; García-Labiano, F.; Gayán, P.; Celaya, J.; Palacios, J. M.; and Adánez, J. Operation of a 10kWth chemical-looping combustor during 200 h with a CuO–Al2O3 oxygen carrier. *Fuel*, **2007**, 86(7–8), 1036.

(13) Adánez, J.; Gayán, P.; Celaya, J.; de Diego, L. F.; García-Labiano, F.; and Abad, A. Chemical looping combustion in a 10 kWth prototype using a CuO/Al2O3 oxygen carrier:effect of operating conditions on methane combustion. *Ind Eng Chem Res*. **2006**, 45(17), 6075.

(14) Johansson, E.; Mattisson, T.; Lyngfelt, A.; and Thunman, H. Combustion of syngas and natural gas in a 300W chemical-looping combustor. *Chem. Eng. Res. Des*. **2006**, 84(A9), 819.

(15) Abad, A.; Mattisson, T.; Lyngfelt, A.; and Johansson, M. The use of iron oxide as oxygen carrier in a chemical-looping reactor. *Fuel*, **2007**, 86(7–8), 1021.

(16) Linderholm, C.; Abad, A.; Mattisson, T.; and Lyngfelt, A. 160 hours of chemical-looping combustion in a 10 kW reactor system with a NiO-based oxygen carrier. *Int. J. Greenhouse Gas Control*, **2008**, 2(4), 520.

(17) Pröll, T.; Kolbitsch, P.; Bolhàr-Nordenkampf, J.; and Hofbauer, H. A dual circulating fluidized bed (DCFB) system for chemical looping processes. In: Proceedings of AIChE annual meeting. Philadelphia, USA; 2008.

(18) Lyngfelt, A.; Johansson, M.; and Mattisson, T. Chemical-looping combustion – status of development. In: Proceedings of 9th international conference on fluidized bed (CFB-9). Hamburg, Germany; 2008.

(19) Hossain, M. M.; and de Lasa, H. I. Chemical-looping combustion (CLC) for inherent CO_2 separations – a review. *Chem. Eng. Sci*., **2008**, 63(18), 4433.

(20) Beatrız, M.; Corbella, J.; and Marıa, P. Titania-supported iron oxide as oxygen carrier for chemical-looping combustion of methane", *Fuel*, **2007**, 86, 113.

(21) Cho, P.; Mattison, T.; and Lyngfelt, A. Comparison of iron, nickel, copper and manganese –based oxygen carriers for chemical-looping combustion. *Fuel*, **2004**, 83, 1215.

(22) Ishida, M.; and Okamoto, T. A. A fundamental study of a new kind of medium material for chemical-looping combustion. *Energy Fuels*, **1996**, 10, 958.

(23) Ishida, M.; Yamamoto, M.; and Ohba, T. Experimental results of chemical looping
combustion with NiO/NiAl2O4 particle circulation at 1200 ^{o}C. *Energ. Convers. Manage*. **2002**, 43, 1469.

(24) Adánez, J.; de Diego, L. F.; García-Labiano, F.; Gayán, P.; Abad, A.; and Palacios, J. M. Selection of oxygen carriers for chemical-looping combustion. *Energy Fuels* **2004**, 18, 371.

(25) Zafar, Q.; Mattison, T.; and Gevert B. Integrated hydrogen and power production with CO2 capture using chemical-looping reforming redox reactivity of particles of CuO, Mn2O3, NiO and Fe2O3 using SiO2 as a support. *Ind. Eng. Chem. Res*. **2005**, 44, 3485.

(26) Monazam, E. R.; Breault, R. W.; Siriwardane, R.; Richards, G.; and Carpender, S. Kinetics of the reduction of hematite (Fe_2O_3) by methane (CH_4) during chemical looping combustion: a global mechanism. *Chem. Eng. J.* **2013**, CEJ-D-13-01232R2.

(27) Miller, D. D.; and Siriwardane, R. Mechanism of methane chemical looping combustion with hematite promoted with CeO2. *Energy Fuels* **2013**; ef302132e.

(28) Cho, P.; Mattisson, T.; and Lyngfelt, A. Carbon formation on nickel and iron oxide containing oxygen carriers for chemical-looping combustion. *Ind. Eng. Chem. Res.* **2005**, 44(4), 668.

(29) Janković , B.; Adnađević, B.; Jovanović, J. Application of model-fitting and model-free kinetics to the study of non-isothermal dehydration of equilibrium swollen poly (acrylic acid) hydrogel: Thermogravimetric analysis Thermochimica Acta **2007**,452, 106–115.

(30) Vyazovkin, S. A unified approach to kinetic processing of nonisothermal data. *Int. J. Chem.* Kinet. **1996**, 28, 95.

(31) Vyazovkin, S. Conversion dependence of activation energy for model DSC curves of consecutive reactions. *Thermochim Acta*. **1994**, 236, 1.

(32) Velisaris, C. N.; and Sefeis, J. C. Crystallization kinetics of polyetheretherketone (PEEK) matrices. *Polym. Eng. Sci*. **1986**, 26, 1574.

(33) Abad, A.; Adánez, J.; García-Labiano, F.; de Diego, L. F.; Gayán, P.; and Celaya, J. Mapping of the range of operational conditions for Cu-, Fe-, and Ni-based oxygen carriers in chemical-looping combustion, *Chem. Eng. Sci*. **2007**, 62, 533.

(34) Moghtaderi, B.; and Song, H. Reduction properties of physically mixed metallic oxide oxygen carriers in chemical looping combustion *Energy Fuels* **2010**, 24, 5359.

Table 1. BET surface areas of oxygen carriers.

Carrier	Fresh (m^2/g)	Reacted[a] (m^2/g)	Fresh Pore Size[b]	Reacted[a] (Å)
MgO (hydroxide)	13.3	-	99.9	-
MgO (nitrate)	4.1	-	193.2	-
Dolomite	< 1.0	-	136.1	-
Fe_2O_3 (Hematite)	< 1.0	< 1.0	63.6	79.7
5% Al_2O_3/Fe_2O_3	1.3	< 1.0	67	-
25% Al_2O_3/Fe_2O_3	1.6	< 1.0	129.4	-
5% MgO(nitrate)/Fe_2O_3	< 1.0	< 1.0	150.9	162.1
25% MgO(nitrate)/Fe_2O_3	2.6	1.4	206.1	182.4
5% MgO(hydroxide)/Fe_2O_3	< 1.0	< 1.0	290.8	141.0
25% MgO(hydroxide)/Fe_2O_3	4.1	1.4	306.1	219.6
5% Dolomite/Fe_2O_3	< 1.0	< 1.0	689.5	161.8
25% Dolomite/Fe_2O_3	1.6	< 1.0	567.3	196.2

[a] *Reaction temperature 800 C*
[b] *Freshly prepared materials*

Table 2. The basic kinetic models and properties of *f(X)* and *g(X)* functions [29].

No.	Symbol	Kinetic Model	*f(X)*	*g(X)*
1	P1	Power Law	$4X^{3/4}$	$X^{1/4}$
2	P2		$3X^{2/3}$	$X^{1/3}$
3	P3		$2X^{1/2}$	$X^{1/2}$
4	P4		$2/3X^{-1/2}$	$X^{3/2}$
		Contraction Model,		
5	R1	Zero order	1	X
6	R2	2-D	$2(1-X)^{1/2}$	$[1-(1-X)^{1/2}]$
7	R3	3-D	$3(1-X)^{2/3}$	$[1-(1-X)^{1/3}]$
		Kinetics-order models,		
8	F1	1st order	$(1-X)$	$-ln(1-X)$
9	F3/2	3/2 order	$(1-X)^{3/2}$	$2[(1-X)^{-1/2}-1]$
10	F2	2nd order	$(1-X)^{2}$	$(1-X)^{-1}-1$
11	F3	3rd order	$(1-X)^{3}$	$1/2[(1-X)^{-2}-1]$
		Nucleation Model,		
12	A3/2	n=1.5	$3/2(1-X)[-ln(1-X)]^{1/3}$	$[-ln(1-X)]^{2/3}$
13	A2	n=2	$2(1-X)[-ln(1-X)]^{1/2}$	$[-ln(1-X)]^{1/2}$
14	A3	n=3	$3(1-X)[-ln(1-X)]^{2/3}$	$[-ln(1-X)]^{1/3}$
15	A4	n=4	$4(1-X)[-ln(1-X)]^{3/4}$	$[-ln(1-X)]^{1/4}$
		Diffusion model,		
16	D1	1-D	$1/(2X)$	X^{2}
17	D2	2-D	$1/[-ln(1-X)]$	$(1-X)ln(1-X)+X$
18	D3	3-D (Jander)	$(3/2)(1-X)^{2/3}[1-(1-X)^{1/3}]$	$[1-(1-X)^{1/3}]^{2}$
19	D4	3-D(Grinstling)	$(3/2)[(1-X)^{-1/3}-1]$	$(1-2X/3)-(1-X)^{2/3}$

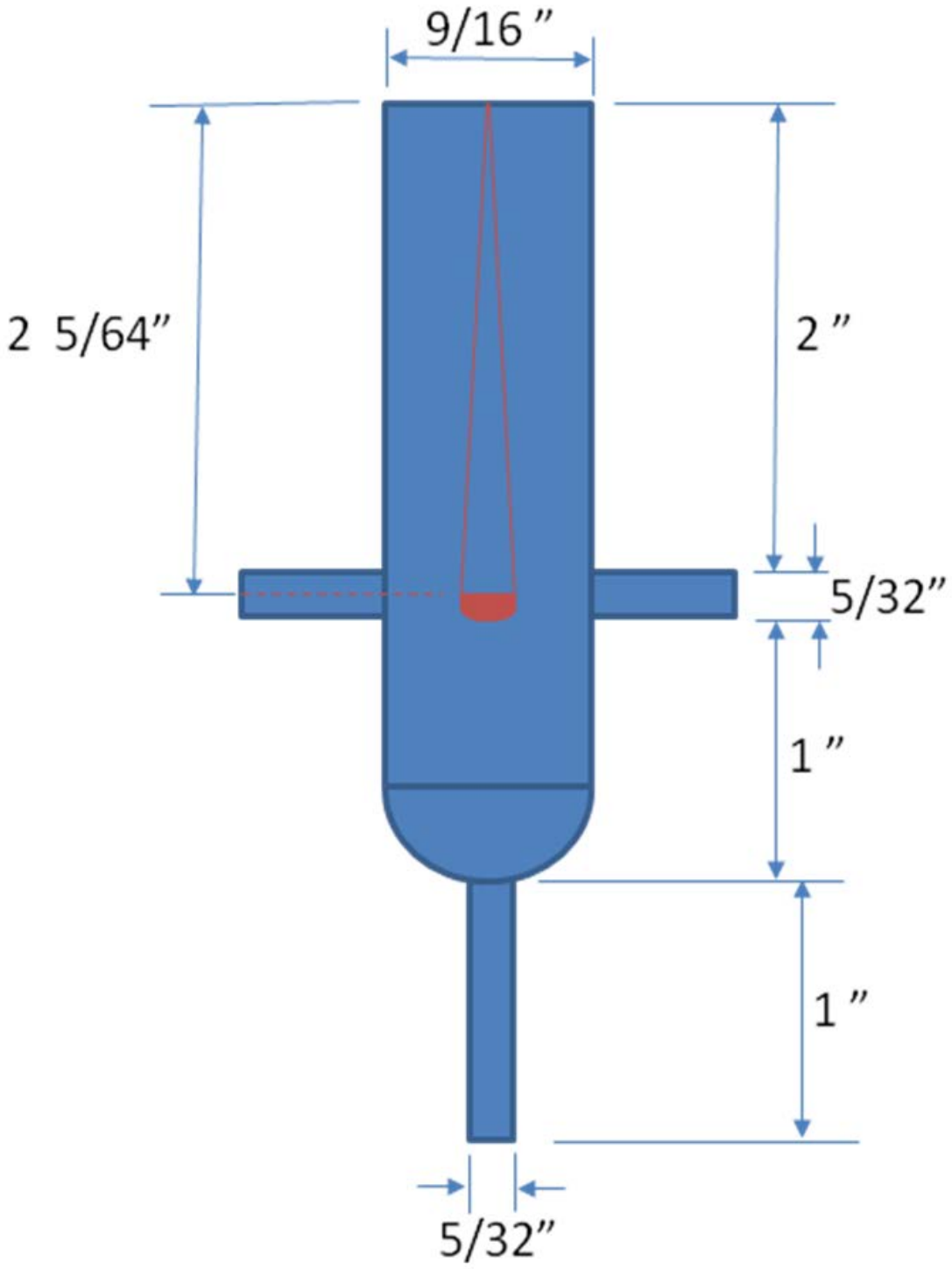

Figure 1 – Sketch of TA Model 2050 thermo gravimetric analyzer

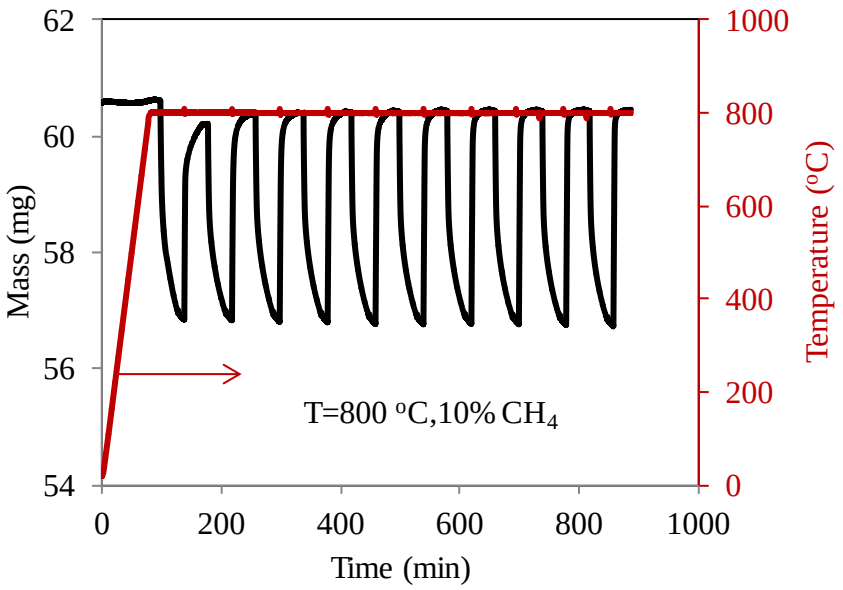

Figure 2. Typical mass and temperature measurement for modified hematite particle of 80 μm using 10% CH_4 for reduction and air for oxidation reactions.

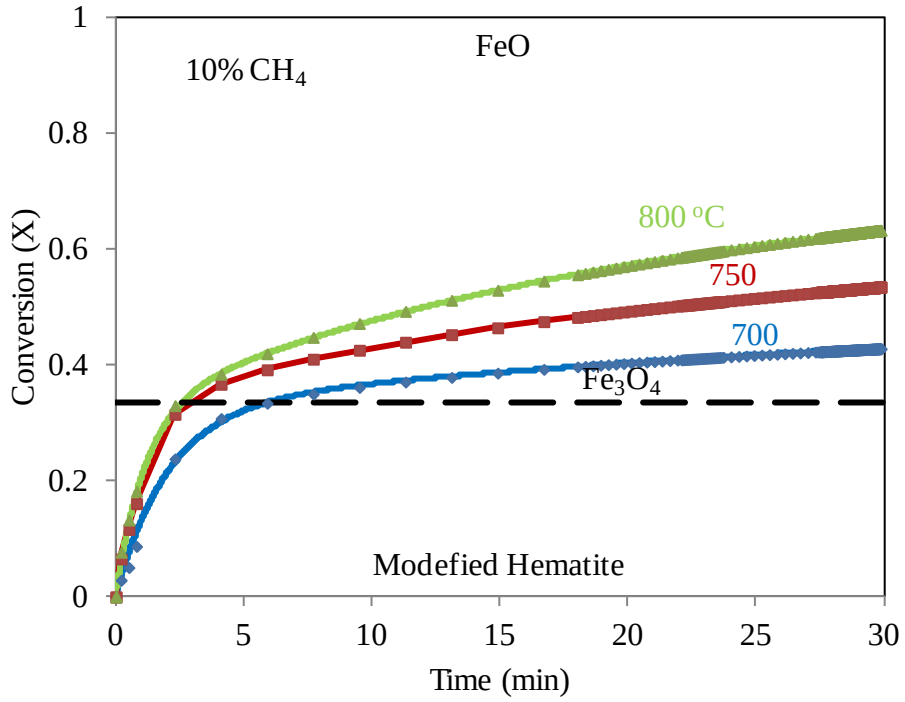

Figure 3. Effect of reaction temperature on conversion of modified hematite to FeO using 10% CH_4.

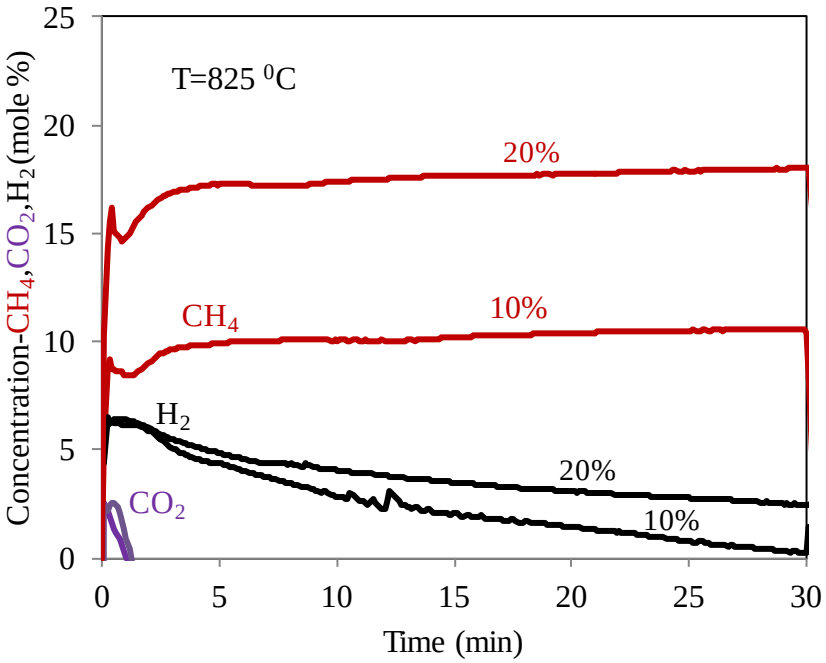

Figure 4. Outlet gas analysis for the reduction of modified hematite (Fe_2O_3) with methane (20 and 10% CH_4) using a reaction temperature of 825 °C.

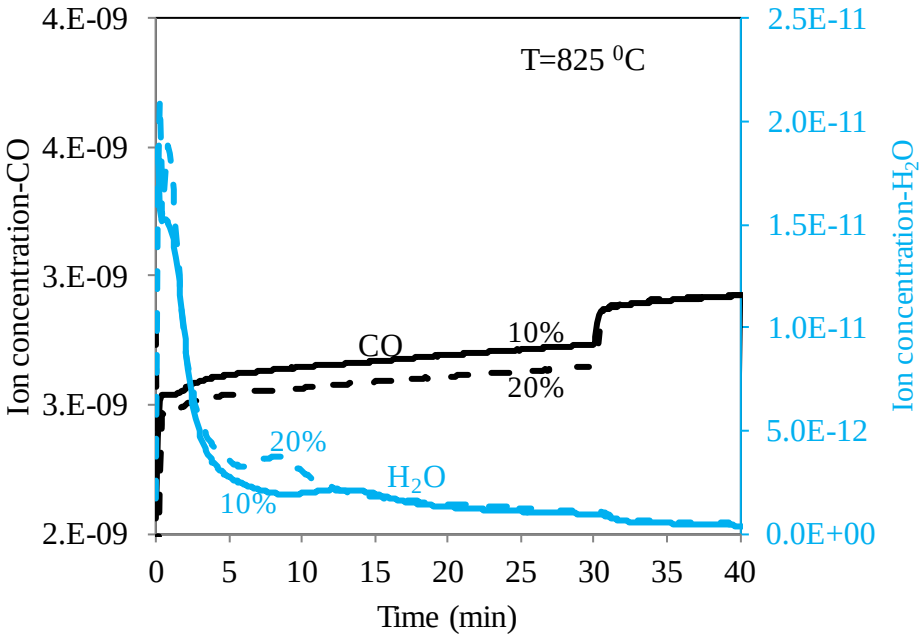

Figure 5. Mass spectral (ion current) of H_2O and CO_2 for the reduction of modified hematite (Fe_2O_3) with methane (20 and 10% CH_4) using a reaction temperature of 825 °C.

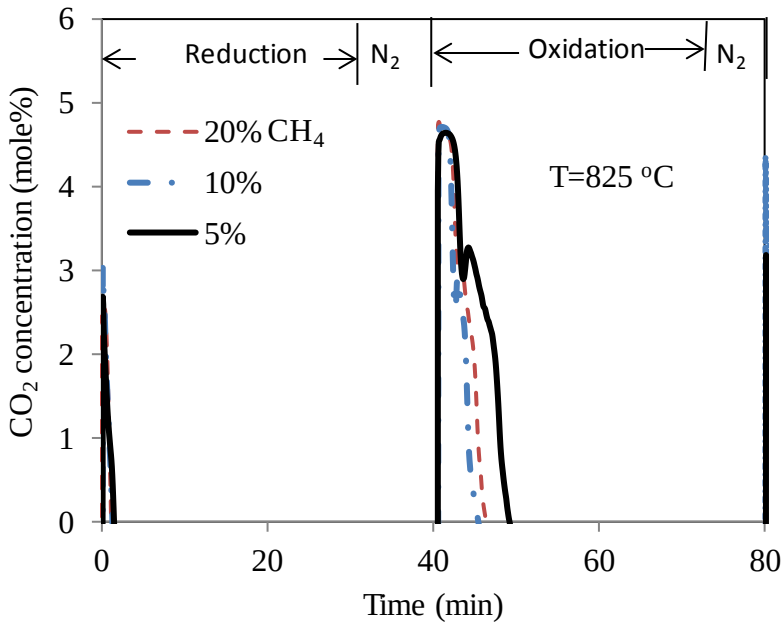

Figure 6. Effect of CH4 concentration on CO_2 concentration during reduction and oxidation of modified hematite.

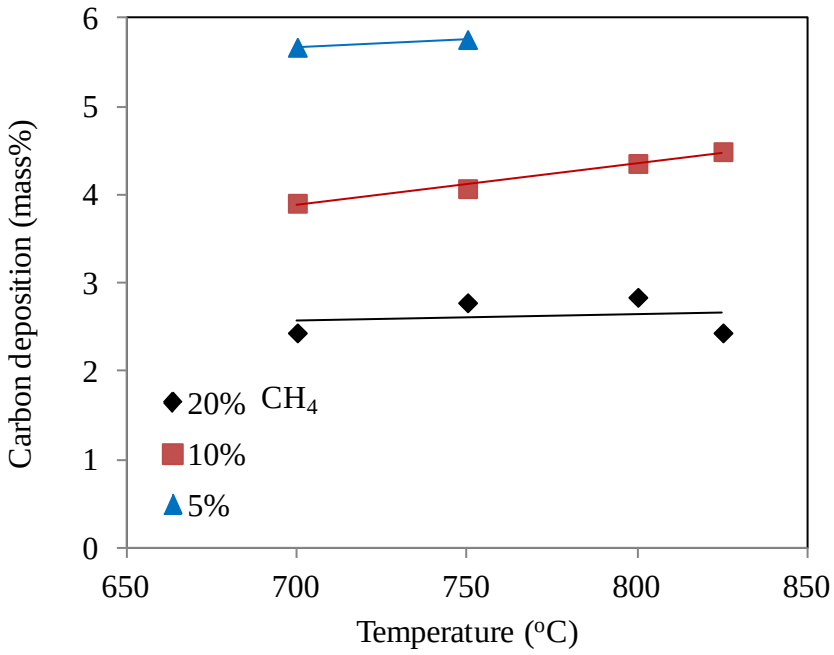

Figure 7. Carbon contents in reduced hematite for different temperature and CH_4 concentrations (5%, 10% and 20%).

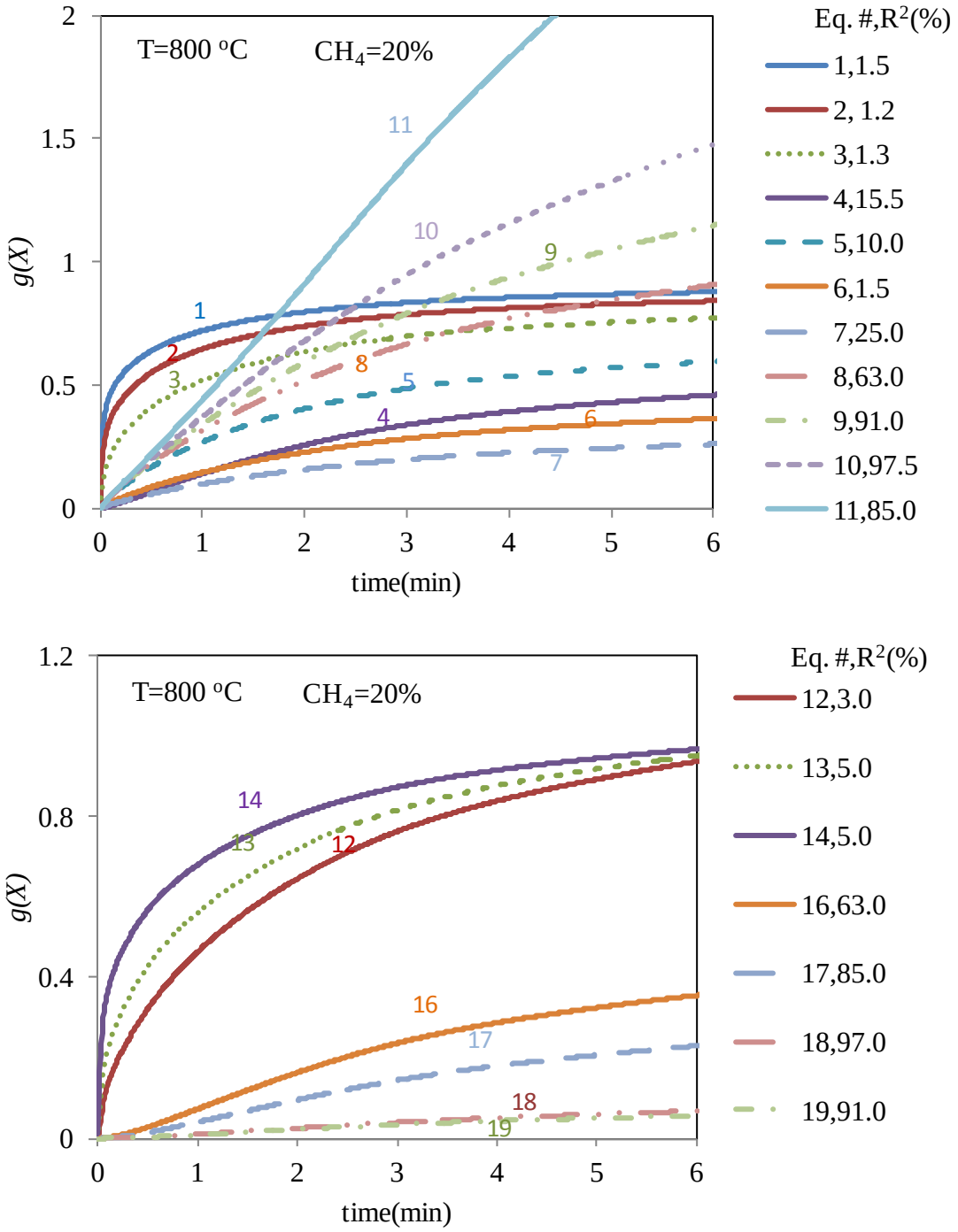

Figure 8. Examination of linear relationship for different reaction models.

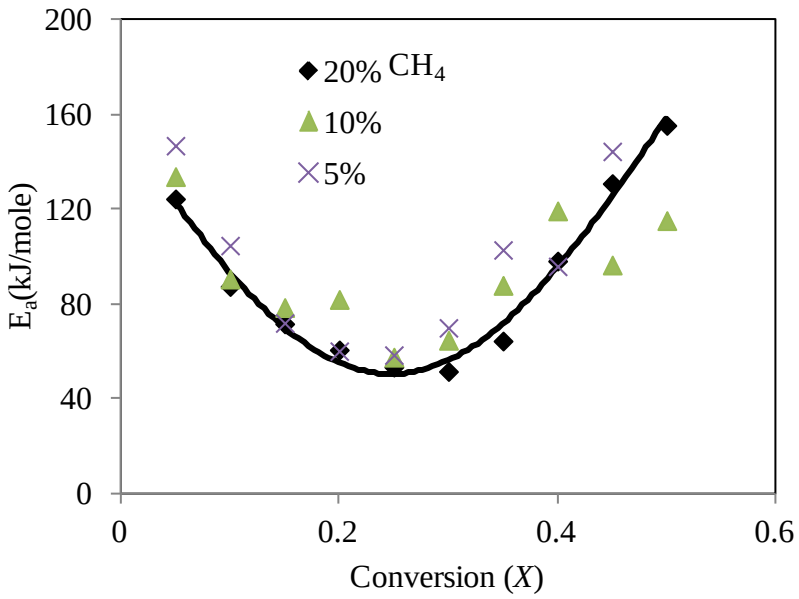

Figure 9. Activation energy values as a function of *X* obtained by an isothermal isoconversional method using CH_4 concentration of 5%, 10% and 20%..

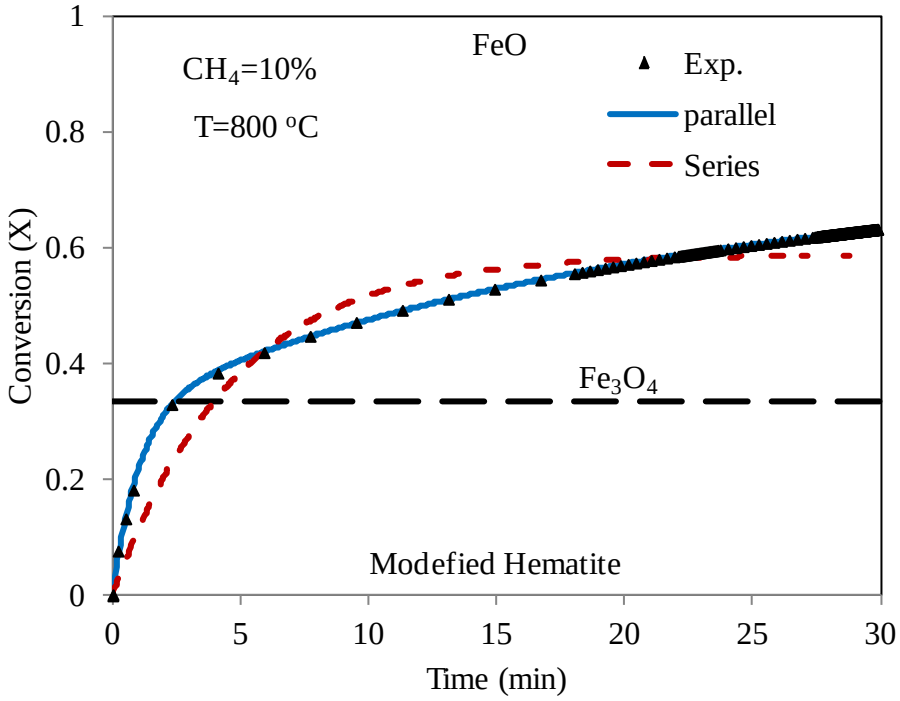

Figure 10. Typical curve fitting of experimental reduction data using series and parallel reactions for 10% methane and 800 °C.

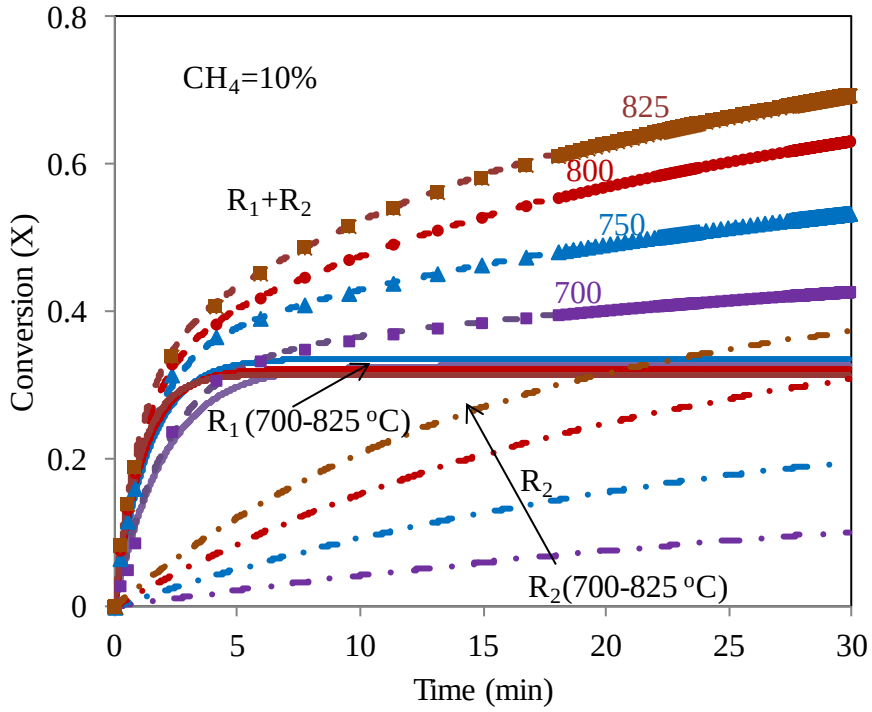

Figure 11. Three predicted curves of conversion as a function of time during isothermal reaction of modified Fe_2O_3 with 10% CH_4. Curve R_1: single 1st order reaction; curve R_2: single 1st order equation; curve R_1+R_2: parallel reaction representing the sum of curve R_1 and R_2. Symbols are experimental data.

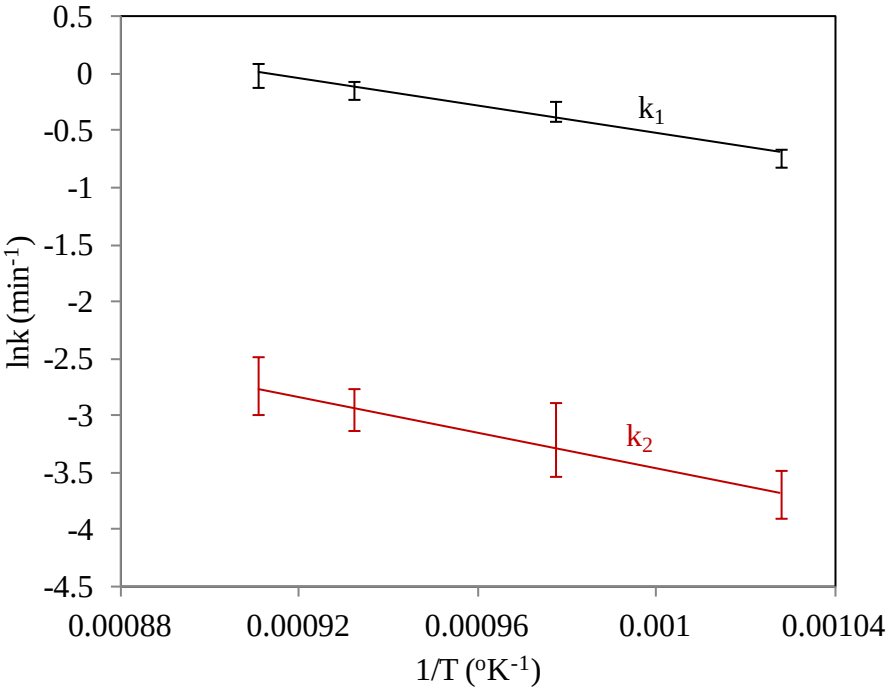

Figure 12. Temperature dependence of the reaction rate, k (min^{-1}), for two parallel reactions for all CH_4 concentrations. Error bars are defined by data range.

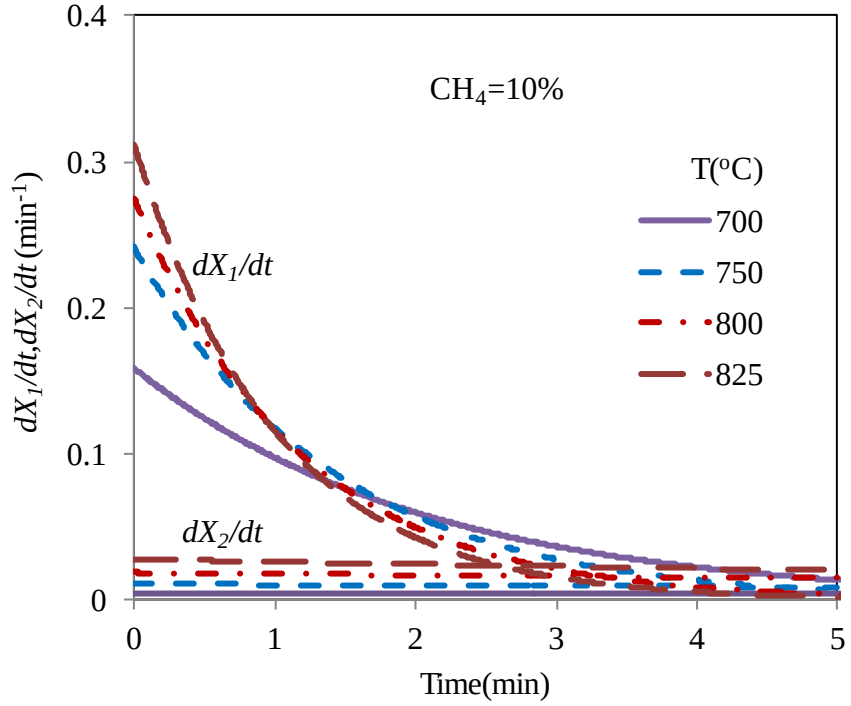

Figure 13. Effect of reaction temperature on the rate of reduction of hematite particle with 20% CH_4 reaction.

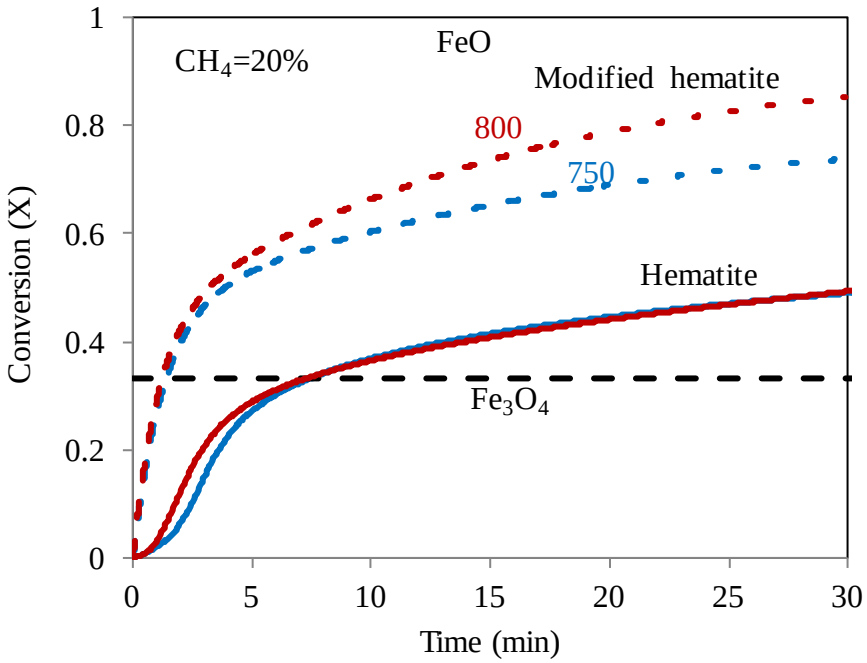

Figure 14. Enhancement achieved with the Mg-modified hematite by observing the degree of reduction between Mg-modified hematite and unmodified hematite using 20% methane at 750 and 800°C.